Universal Breakdown of Elasticity at the Onset of Material Failure

Craig Maloney[1,2] and Anaël Lemaître[1,3]
[1]*Department of Physics, University of California, Santa Barbara, California 93106, USA*
[2]*Lawrence Livermore National Lab, CMS-MSTD, Livermore, California 94550, USA*
[3]*LMDH, Universite Paris VI, UMR 7603, 4 place Jussieu, 75005 Paris, France*
(Received 6 May 2004; published 2 November 2004)

We show that, in the athermal quasistatic deformation of amorphous materials, the onset of failure is accompanied by universal scalings associated with a *divergence* of elastic constants. A normal mode analysis of the nonaffine elastic displacement field allows us to clarify its relation to the zero-frequency mode at the onset of failure and to the cracklike pattern which results from the subsequent relaxation of energy.

DOI: 10.1103/PhysRevLett.93.195501 PACS numbers: 62.20.Dc, 62.20.Fe, 62.25.+g, 72.80.Ng

Experiments on nanoindentation of metallic glasses [1], on granular materials [2] and on foams [3], demonstrate that at very low temperature and strain rates the microstructural mechanisms of deformation involve highly intermittent stress fluctuations. These fluctuations can be accessed in molecular dynamics simulations, but are best characterized numerically via "exact" implementation of athermal quasistatic deformation: alternating elementary steps of affine deformation with energy relaxation [4] permits one to constrain the system to reside in a local energy minimum (inherent structure) at all times. As illustrated in Fig. 1, macroscopic stress fluctuations arise from a series of reversible (elastic) branches corresponding to deformation-induced changes of local minima. These branches are interrupted by sudden irreversible (plastic) events which occur when the inherent structure annihilates during a collision with a saddle point [5]. These transitions constitute the most elementary mechanism of deformation and failure for disordered materials at low temperature.

Using this quasistatic protocol, recent studies of both elasticity [6] and plasticity [5] could identify important properties of elastoplastic behavior which arise solely from the geometrical structure of the potential energy landscape. Tanguy *et al.* [6] have observed that, following *reversible* (elastic) changes of the inherent structures, molecules undergo large scale nonaffine displacements. They have shown these nonaffine displacements to be related to the breakdown of classical elasticity at small scales and to quantitative differences between measured Lamé constants and their Born approximation. Malandro and Lacks [5] have shown that the destabilization of a minimum occurs through shear-induced collision with a saddle. At the collision, a single normal mode sees its eigenvalue going to zero. Building on this work, we studied the *irreversible* (plastic) event following the disappearance of an inherent structure: subsequent material deformation in search of a new minimum involves nonlocal displacement fields—in the likeness of nascent cracks—controlled by long-range elastic interactions [7].

Several molecular displacement fields thus appear to be closely related to the geometrical structure of the potential energy landscape: (i) nonaffine displacements along elastic branches, (ii) the single normal mode controlling the annihilation of an inherent structure, and (iii) the overall deformation occurring during an irreversible event. In order to piece together a complete picture of elastoplasticity at the nanoscale, we need to understand the relation between these different fields and ask how elastic behavior breaks down at the onset of failure. It is thus a study of incipient plasticit, *the onset of irreversible deformation*, that we wish to perform. Here the structural disorder is expected to control the onset of failure: this situation is somehow opposite to homogeneous defect nucleation in crystals [8], where failure is controlled by Hill's continuum condition [9].

We base our approach on exact microscopic expressions for the nonaffine corrections to elasticity in disordered solids [10,11], which have been entirely overlooked in recent works. Here we put such analytical tractations in perspective with the recent numerical developments. We derive an exact formulation for the nonaffine displace-

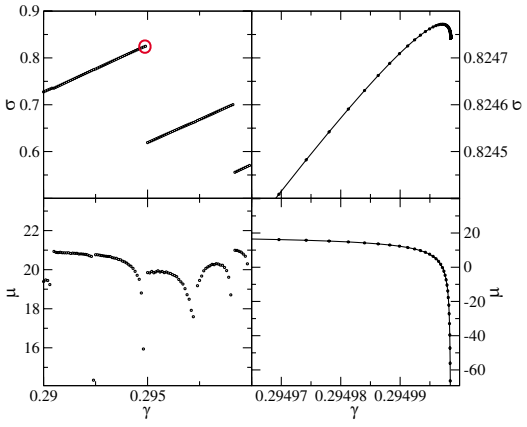

FIG. 1 (color online). Stress (top) and shear modulus (bottom) for a small strain interval about a strain of 0.3. Left: Fixed strain steps of size 10^{-4}. Right: Convergence to the yield point.

ment fields, and construct a normal mode decomposition therefrom. This analytical framework permits us to evidence that the lowest frequency normal mode dominates the nonaffine elastic displacement field close to a plastic transition. We then show that at any plastic transition point, the mechanical properties display a singular, universal behavior associated with a *divergence* of the elastic constants. A normal mode analysis of the subsequent cascade shows that the entire reconfiguration is dominated by the low frequency modes only in its early stages.

We consider a molecular system in a periodic cell. The geometry of the cell is determined by the matrix h whose columns are the Bravais vectors [12,13]. The affine deformation of the cell between configurations h_0 and h is characterized by the Green-St. Venant strain tensor, $\underline{\underline{\epsilon}} = \frac{1}{2}[(h_0^{-1})^T \cdot h^T \cdot h \cdot h_0^{-1} - 1]$, which governs the elongation of a vector $\mathring{\vec{x}} \rightarrow \vec{x}$, as $\vec{x}^2 = \mathring{\vec{x}}^2 + 2\mathring{\vec{x}}^T \cdot \underline{\underline{\epsilon}} \cdot \mathring{\vec{x}}$. As the energy functional generally depends only on the set of interparticle distances, it can be parametrized as $\mathcal{U}(\{\mathring{\vec{r}}_i\}, \underline{\underline{\epsilon}})$, where $\{\mathring{\vec{r}}_i\}$ are the positions of the particles in a *reference* cell [10,14]. Varying $\underline{\underline{\epsilon}}$ for fixed $\{\mathring{\vec{r}}_i\}$ corresponds to an affine displacement of the molecules in real space.

To start, let us contemplate more closely the athermal, quasistatic algorithm. Deformation, $\underline{\underline{\epsilon}}(\gamma)$, is enforced by moving the Bravais axes of the periodic cell; γ is introduced as a rescaled coordinate to measure the deformation from some reference state. In practice, $\underline{\underline{\epsilon}}(\gamma)$ corresponds to either pure shear or pure compression. Formally, the limit $h_0 = h$ (or $\gamma \rightarrow 0$) is often appropriate to define stresses and elastic constant around a (possibly stressed) reference state. Once a choice of h_0 is made, the algorithm tracks in the reference cell a trajectory $\{\mathring{\vec{r}}_i\}(\gamma)$, which is implicitly defined by demanding that the system remain in mechanical equilibrium [10,11]:

$$\forall\ i, \qquad \vec{F}_i \equiv \frac{\partial \mathcal{U}}{\partial \mathring{\vec{r}}_i}\ \Big|_{\gamma}\ (\{\mathring{\vec{r}}_j\}, \gamma) = \vec{0}. \tag{1}$$

Starting at mechanical equilibrium at $\gamma = 0$, $\{\mathring{\vec{r}}_i(\gamma)\}$ is a continuous function of γ on some interval $[0, \gamma_c]$. At γ_c, the local minimum collides with a saddle point. [5]

An equation of motion for $\mathring{\mathbf{r}} = \{\mathring{\vec{r}}_i(\gamma)\}$ is obtained by derivation of (1) with respect to γ. Denoting $\mathcal{H} = (\partial^2 \mathcal{U}/\partial \mathring{\vec{r}}_i \partial \mathring{\vec{r}}_j)$, $\vec{\Xi} = (\partial^2 \mathcal{U}/\partial \mathring{\vec{r}}_i \partial \gamma)$, and $\vec{\Xi}_{\alpha\beta} = (\partial^2 \mathcal{U}/\partial \mathring{\vec{r}}_i \partial \epsilon_{\alpha\beta})$, we find

$$\frac{d\mathring{\mathbf{r}}}{d\gamma} = -\mathcal{H}^{-1} \cdot \vec{\Xi} = -\mathcal{H}^{-1} \cdot \sum_{\alpha\beta} \vec{\Xi}_{\alpha\beta} \frac{d\epsilon_{\alpha\beta}}{d\gamma}. \tag{2}$$

This relation holds for any $\gamma \in [0, \gamma_c]$. In the limit $h \rightarrow h_0$, $\mathcal{H}$ is the dynamical matrix. To invert $\mathcal{H}$, translation modes must be eliminated by fixing the position of a molecule. $d\mathring{\mathbf{r}}/d\gamma$ is a rescaled "velocity" of molecules in quasistatic deformation. It defines the direction (in tangent space) of the nonaffine displacement field observed by Tanguy *et al.* and can be directly evaluated by solving Eq. (2) without resorting to quadruple precision minimization [6].

Here, we illustrate these ideas with numerical simulations of a two-dimensional bidisperse mixture of particles interacting through a shifted Lennard-Jones potential [6]. Particle sizes $r_S = r_L \sin\frac{\pi}{10} / \sin\frac{\pi}{5}$ and a number ratio $N_L/N_S = \frac{1+\sqrt{5}}{4}$ are used to prevent crystallization; the simulation cell is $50 \times r_L$ in length, yielding 4938 particles. We have also performed simulations on Hertzian spheres to check that it yielded results consistent with those presented here. Typical patterns of the fields $\vec{\Xi}$ and $d\mathring{\mathbf{r}}/d\gamma$ in (steady) simple shear deformation are shown Fig. 2: the apparent small scale randomness of the vector $\vec{\Xi}$ is in sharp contrast with the large vortexlike structures displayed by the nonaffine velocity field $d\mathring{\mathbf{r}}/d\gamma$. To understand the randomness of $\vec{\Xi}$, note that $\vec{\Xi}_i = \partial \vec{F}_i/\partial\gamma$ is the force response on molecule i after an elementary affine deformation of the system: it depends only on the configuration of the molecules with which molecule i interacts, hence an $\underline{\underline{\epsilon}}$-dependent measure of the local disorder of molecular configurations. We checked that spatial correlations decay very fast in the field $\vec{\Xi}$: in the following discussion, the short-range randomness of the field $\vec{\Xi}$ allows us to interpret it as noise.

An analytical expression for the bulk elastic constants derives along similar lines [10,11]. The first derivative of the potential with respect to the components of $\underline{\underline{\epsilon}}$ defines the thermodynamic stress, $\underline{\underline{t}}$: $t_{\alpha\beta} = \frac{1}{V_0}\frac{d\mathcal{U}}{d\epsilon_{\alpha\beta}} = \frac{1}{V_0}\frac{\partial \mathcal{U}}{\partial \epsilon_{\alpha\beta}}$. The total derivative indicates derivation while preserving mechanical equilibrium, the second equality results from Eq. (1), and V_0 is the volume of the simulation cell. The second (total) derivative of the energy gives the elastic constants [14]:

$$C_{\alpha\beta\chi\sigma} = \frac{1}{V_0}\left(\frac{\partial^2 \mathcal{U}}{\partial \epsilon_{\alpha\beta} \partial \epsilon_{\chi\sigma}} + \sum_j \frac{\partial^2 \mathcal{U}}{\partial \mathring{\vec{r}}_i \partial \epsilon_{\alpha\beta}} \cdot \frac{d\mathring{\vec{r}}_i}{d\epsilon_{\chi\sigma}}\right). \tag{3}$$

We recognize the first term as being the Born approximation $C^{\text{Born}}_{\alpha\beta\chi\sigma}$. The second term accounts for the nonaffine corrections, and reads $\tilde{C}_{\alpha\beta\chi\sigma} = -\frac{1}{V_0}\vec{\Xi}_{\alpha\beta} \cdot \mathcal{H}^{-1} \cdot \vec{\Xi}_{\chi\sigma}$. Similarly, the second derivatives of the energy,

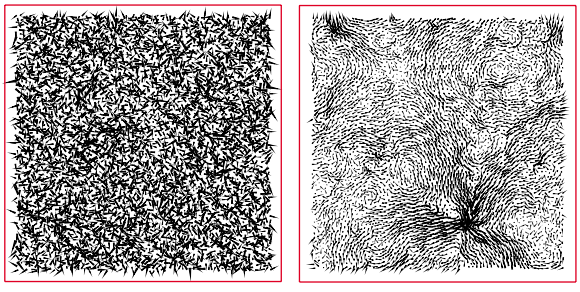

FIG. 2 (color online). Left: The force response to simple shear, $\vec{\Xi}$, at a strain configuration, $\gamma = 0.2945$, or $\gamma_c - \gamma \sim 10^{-4}$. Right: The nonaffine velocity (or "displacement") field, $\frac{d\mathring{\mathbf{r}}}{d\gamma}$ for the same state as shown on the left.

following any generic deformation $\underline{\epsilon}(\gamma)$, can be written as

$$\frac{d^2U}{d\gamma^2} = \frac{\partial^2 U}{\partial \gamma^2} - \vec{\Xi} \cdot \mathcal{H}^{-1} \cdot \vec{\Xi}. \quad (4)$$

For an isotropic material, the elastic constants can be written as $C_{\alpha\beta\chi\sigma} = \lambda\delta_{\alpha\beta}\delta_{\chi\sigma} + \mu(\delta_{\alpha\chi}\delta_{\beta\sigma} + \delta_{\alpha\sigma}\delta_{\beta\chi})$, which define the Lamé constants λ and μ. In order to estimate these constants, it is not necessary to evaluate all the components of the tensor $\vec{\Xi} = (\vec{\Xi}_{\alpha\beta})$, but only two of its projections $\vec{\Xi}$, e.g., for pure shear and pure compression, and use Eq. (4). In Eq. (4) the correction to the Born term is negative definite: quantities such as the shear modulus, μ, or the compressibility, $K = \lambda + \mu$, are necessarily smaller than the Born term, while this is not necessarily true of $\lambda = K - \mu$ alone as it does not, by itself, correspond to any realizable mode of deformation. This is consistent with the numerical observations by Tanguy *et al.* [6] in Lennard-Jones systems.

Next, we perform a normal mode analysis of the fields $\vec{\Xi}$. Denoting $\vec{\Psi}_p$ the eigenvectors of the dynamical matrix (normal modes), and λ_p the associated eigenvalues, the vector $\vec{\Xi}$ can be decomposed as $\vec{\Xi} = \sum_p \xi_p \vec{\Psi}_p$, with $\xi_p = \vec{\Xi} \cdot \vec{\Psi}_p$. (If $\vec{\Xi}$ is a random field, the variables ξ_p are random.) From this decomposition, expressions can be obtained for the nonaffine direction and for the nonaffine contribution to elasticity:

$$\frac{d\mathring{\mathbf{r}}}{d\gamma} = -\sum_p \frac{\xi_p}{\lambda_p}\vec{\mathbf{\Psi}}_p \quad \text{and} \quad C_{\underline{\epsilon}} = -\sum_p \frac{\xi_p^2}{\lambda_p}. \quad (5)$$

We now concentrate on the behavior of the shear modulus at incipient plasticity, as shown in Figs. 1 and 3. Malandro and Lacks have shown numerically that at the onset of a plastic event a single eigenfrequency goes to zero [5]. We denote $\vec{\Psi}^*(\gamma)$ the first nonzero normal mode; in two dimensions, it is the third in the spectrum. Close to failure ($\gamma \to \gamma_c$), $\lambda^*(\gamma) \to 0$; hence $\vec{\Psi}^*(\gamma_c)$ must dominate the nonaffine direction $d\mathring{\mathbf{r}}/d\gamma$. This is true if and only if the quantity $\xi^*(\gamma) = \vec{\Psi}^*(\gamma) \cdot \vec{\Xi}(\gamma)$ does not vanish at the yield point.

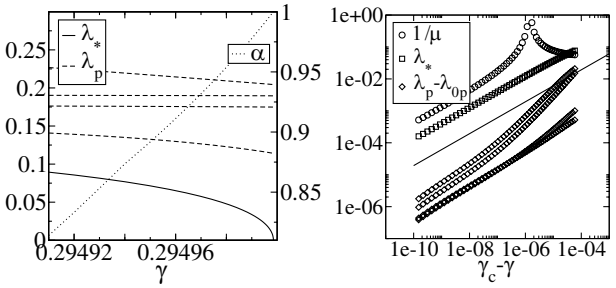

FIG. 3. Left: Relative participation of the lowest normal mode in the nonaffine elastic displacement field, $\alpha^* \doteq (\xi^*/\lambda^*)^2/\sum_p(\xi_p/\lambda_p)^2$ (dotted line); lowest eigenvalue of the dynamical matrix (solid line); next several eigenvalues (dashed line). Right: In log-log scale (as a guide to the eye, the thick black line is $\sqrt{\gamma_c - \gamma}$): $1/\mu$ (circles); lowest eigenvalue (squares); next several eigenvalues minus their terminal values (diamonds).

In order to check this scenario, we have performed numerical simulations of the same 2D binary mixture described above. Minimization was performed using a standard conjugate gradient approach, but by first converging to the local inflection point during the line search to avoid escaping the shrinking basin. Termination occurred when the maximum force was 10^{-8}. We observe that (i) $\vec{\Psi}^*$ is localized close to failure, while (ii) $\vec{\Xi}(\gamma) \to \vec{\Xi}(\gamma_c)$ remains noisy and weakly correlated with the normal modes. As a consequence of this observation, $\xi^*(\gamma)$ has a random but typically nonzero limit when $\gamma \to \gamma_c$. The nonaffine field is dominated by $-\xi^*(\gamma_c)/\lambda^*(\gamma) \times \vec{\Psi}^*(\gamma_c)$ and the nonaffine correction to elasticity by $\tilde{\mu} \sim -(\xi^*)^2/\lambda^*$, which diverges toward $-\infty$ (see Fig. 1). In contrast, the Born term, which depends on the pair correlation only, does not diverge. Since $\mu = \mu^{\text{Born}} + \tilde{\mu}$, on approaching failure, the system reaches a point $\gamma_0 < \gamma_c$ at which $\tilde{\mu} = -\mu^{\text{Born}}$, whence μ vanishes. For $\gamma \in [\gamma_0, \gamma_c]$, the shear stress is a decreasing function of γ: the material is unstable to any constant applied stress. This region is accessible to us because deformation—and not stress—is prescribed.

In order to understand more specifically how the elastic constants behave close to γ_c, let us consider the functions $\lambda_p(\gamma)$, which are continuous on a small interval close to γ_c (the second derivatives of the potential are supposed to be regular). Close to the yield point, γ_c, the deformation is dominated by the lowest normal mode: $\mathring{\mathbf{r}}(\gamma) - \mathring{\mathbf{r}}(\gamma_c) \sim x(\gamma)\vec{\mathbf{\Psi}}^*(\gamma_c)$. (We project the deformation on the mode $\vec{\Psi}^*$ *at* the yield point.) From this relation and (5), we obtain the dominant contribution: $dx/d\gamma \sim -\xi^*(\gamma_c)/\lambda^*(\gamma)$. The coordinate x measures a true displacement in configuration space: we expect that no singular behavior occurs in this rescaled coordinate whence, $\lambda^*(x)$ should vanish regularly, $\lambda^*(x) \sim ax$ close to $x = 0$. Therefore, $x(\gamma) \sim \sqrt{2\xi^*(\gamma_c)(\gamma_c - \gamma)/a}$. This relation controls entirely the behavior of all observables when approaching the yield point: any observable A which behaves regularly as a function of x (any regular function of molecular configurations) "accelerates" close to the yield point: $dA/d\gamma \sim 1/\sqrt{\gamma_c - \gamma}$. In particular, we obtain $d\mathring{\mathbf{r}}/d\gamma \sim \vec{\mathbf{\Psi}}_p/\sqrt{\gamma_c - \gamma}$ and $\lambda^*(\gamma) = \sqrt{2a\xi^*(\gamma_c - \gamma)}$, whence, $\tilde{\mu} \sim -(\xi^*)^{3/2}/\sqrt{2a(\gamma_c - \gamma)}$. We could observe these scalings numerically by a careful approach to the yield point, as shown Fig. 3. A similar divergence is observed for the compression modulus, but with a different prefactor, determined by the normal mode decomposition of the $\vec{\Xi}$ field associated with pure compression.

We now turn to the overall plastic event following failure (see Figs. 4 and 5). We have already shown, in similar atomistic systems, that any single plastic event involves a cascade of local rearrangements [7]. Our preceding work suggested that the overall plastic event was con-

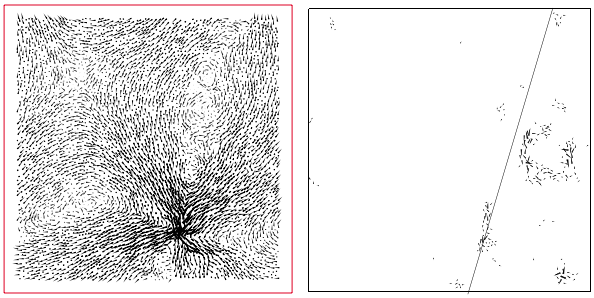

FIG. 4 (color online). Left: Nonaffine elastic displacement field at a distance $\gamma_c - \gamma \sim 10^{-10}$ from the transition. Note the quadrupolar alignment with the direction of applied strain. Right: The local relative displacement field (the displacement of each particle measured with respect to the average displacement of its neighbors) which is incurred after the entire plastic cascade. The solid line is a guide to the eye oriented along the oblique Bravais axis.

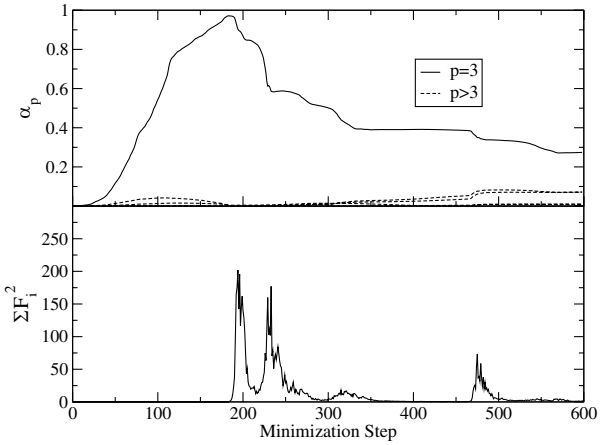

FIG. 5. Evolution of the displacement field during the irreversible cascade corresponding to the event circled in Fig. 1. Top: Contribution α^* (solid line) of the critical mode and $\alpha_p(t)$ (dashed line) of the next five modes to the displacement field. Bottom: Sum of the squares of the forces on the particles.

trolled by long-range elastic interactions and differed from the displacement fields which dominate the onset of failure. Our present normal mode decomposition allows us to gain more insight into this process. Writing $\vec{\mathbf{r}}(t) - \vec{\mathbf{r}}(0) = \sum_p \Delta\xi_p(t)\vec{\Psi}_p(\gamma_c)$, we extract the quantities $\alpha_p \doteq [\Delta\xi_p(t)]^2/\sum_p[\Delta\xi_p(t)]^2$, which are shown Fig. 5 for the lowest frequency modes. To trigger the relaxation, we shear the system forward by a small amount of shear, $\gamma - \gamma_c \sim 10^{-5}$. The initial affine displacement serves as a perturbation and projects randomly on the normal modes, whence the contributions α_p start around zero. We observe that (i) the initiation of the cascade is clearly dominated by the critical mode, (ii) this effect suddenly stops before reaching the first peak in $\sum_i F_i^2$ (this peak corresponds to the first inflection point of energy versus minimization step), and (iii) the subsequent displacement appears to be random, when projected on the lowest part of the spectrum, indicating that low frequency normal modes are irrelevant for the latter stages of plastic failure.

The detailed picture of nascent irreversibility which emerges from our work departs from the traditional viewpoint proposed by Argon and co-workers, which has been the basis of most theoretical approaches for decades [15,16], where elementary events are supposed to be *reversible* and *independent*, irreversibility being expected to arise from the release of stress when, by chance, deformations percolate through neighboring zones. We see here that the transitions between inherent structures are irreversible. Our previous study of the distribution of energy drops during these transitions has shown that the scalings are not consistent with a percolation of independent events: cascades are structured processes comprising *correlated* events [7]. Even if part of the traditional viewpoint may be recovered at nonzero temperatures, the transition between inherent structures is an essential brick in the construction of theories of plasticity. It thus seems that future theories will have to address, at some point, the spatial organization described here, and the *correlated* nature of *irreversible* events.

This work was partially supported under the auspices of the U.S. Department of Energy by the University of California, Lawrence Livermore National Laboratory under Contract No. W-7405-Eng-48, by the NSF under Grants No. DMR00-80034 and No. DMR-9813752, by the W. M. Keck Foundation, and EPRI/DoD through the Program on Interactive Complex Networks. C. M. would like to acknowledge the guidance and support of V.V. Bulatov and J. S. Langer and the hospitality of LLNL University Relations.

[1] C. A. Schuh and T. G. Nieh, Acta Mater. **51**, 87 (2003).
[2] B. Miller, C. OHern, and R. P. Behringer, Phys. Rev. Lett. **77**, 3110 (1996).
[3] E. Pratt and M. Dennin, Phys. Rev. E **67**, 051402 (2003).
[4] K. Maeda and S. Takeuchi, J. Phys. F. Met. Phys. **8**, L283 (1978).
[5] D. L. Malandro and D. J. Lacks, Phys. Rev. Lett. **81**, 5576 (1998); J. Chem. Phys. **110**, 4593 (1999).
[6] A. Tanguy, J. P. Wittmer, F. Leonforte, and J.-L. Barrat, Phys. Rev. B **66**, 174205 (2002).
[7] C. Maloney and A. Lemaître, Phys. Rev. Lett. **93**, 016001 (2004).
[8] J. Li *et al.*, Nature (London) **418**, 307 (2003).
[9] R. Hill, J. Mech. Phys. Solids **10**, 1 (1962).
[10] D. Wallace, *Thermodynamics of Crystals* (Wiley, New York, 1972).
[11] J. F. Lutsko, J. Appl. Phys. **64**, 1152 (1988).
[12] J. Ray and A. Rahman, J. Chem. Phys. **80**, 4423 (1984).
[13] J. R. Ray, M. C. Moody, and A. Rahman, Phys. Rev. B **32**, 733 (1985).
[14] T. Barron and M. Klein, Proc. Phys. Soc. London **85**, 523 (1965).
[15] A. S. Argon, Acta Metall. **27**, 47 (1979).
[16] A. S. Argon and L. T. Shi, Acta Metall. **31**, 499 (1983).